Chapter 8. Kolsky Bar for Dynamic Tensile/Torsion Experiments

In addition to the compression version of the Kolsky bar, there are bars that subject the specimen under tension, torsion, and combined torsion/axial loading conditions to explore the high-rate response of materials under more diversified stress states. The work principles of these bars are similar to that of Kolsky compression bar. However, the loading mechanisms are more complicated than the simple bar-to-bar impact seen in compression experiments. The specimens in both tension and torsion experiments must be attached to the bar ends, which brings in the complication of gage-section identification in strain-rate calculations. This chapter describes various designs of Kolsky bars to conduct dynamic experiments for the specimen stress-strain response under uniaxial tension, pure torsion, combined tension/torsion, or compression/torsion. The designs of specimens will also be described. Examples of high-rate uniaxial tension experiments on polymers, bones, and high-performance fibers are provided.

8.1 Methods to Apply Dynamic Tension on Specimens

Tensile versions of the Kolsky bar started to emerge in 1960's. Harding et al. (1960) developed a method that is schematically shown in Fig. 8.1 to conduct dynamic tension experiments. In their design, the input bar is made of a hollow tube. An elastic bar is attached inside the hollow tube with a yoke connected to the tube end to determine the input loading condition (Fig. 8.1(a)). The specimen assembly shown in Fig. 8.1(b) then replaces the elastic bar for dynamic tension test under the same loading condition. This two-step method was later modified by placing incident and transmission bars with a specimen in between inside the tube for dynamic tensile testing of composites, as shown in Fig. 8.2 (Harding and Welsh 1983). This modified design is nearly the same as the earlier design by Hauser in 1966 as shown in Fig. 8.3. The principle behind these designs is to transfer the external impact into axial tension through an external tube which is connected to the Kolsky-bar system. This approach allows the launching device from a compression bar, i.e. a gas gun, be directly used for the tension bar. However, the entire tension setup is inside a solid tube, which is not efficient in terms of instrumentation (e.g., strain gages on the incident and transmission bar surfaces or temperature sen-

W.W. Chen and B. Song, *Split Hopkinson (Kolsky) Bar: Design, Testing and Applications*, Mechanical Engineering Series, DOI 10.1007/978-1-4419-7982-7_8,

sors on the specimen) and visual observation (e.g., high-speed imaging of the specimen deformation process or optical strain measurements). Other forms of generating tensile loading continue to emerge.

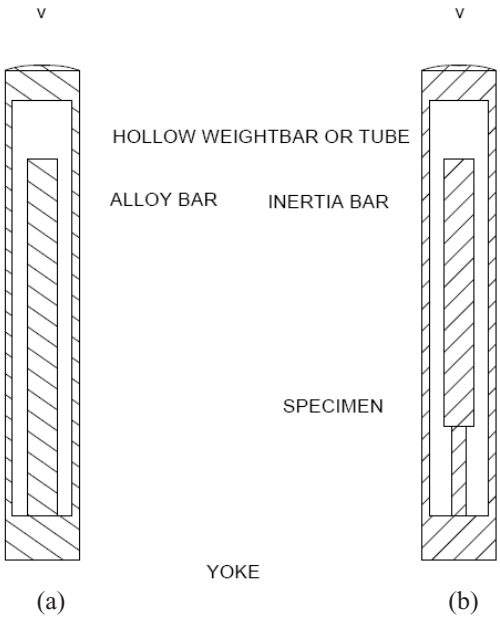

Figure 8.1 An earlier version of tension bar developed by Harding et al. (1960)

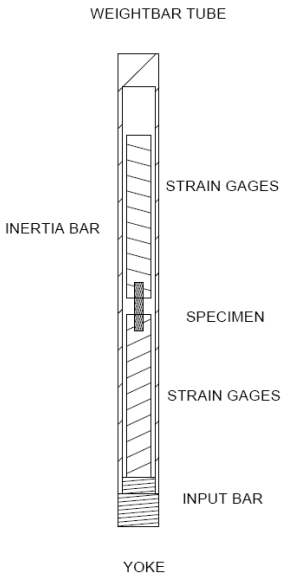

Figure 8.2 A modification of the system by Harding and Welsh (1983)

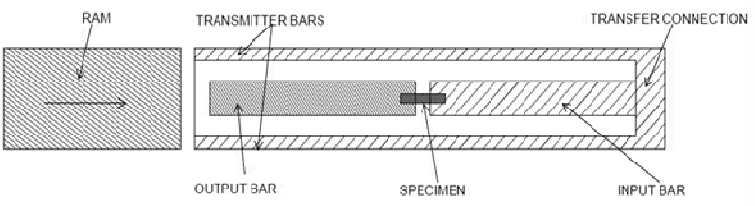

Figure 8.3 Hauser's design of Kolsky tension bar

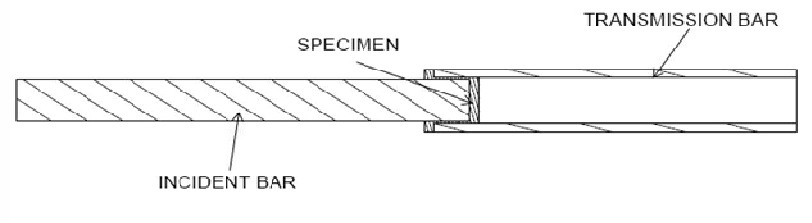

Figure 8.4 A "top-hat" specimen for dynamic tension tests

The simplest modification is a "top-hat" specimen geometry proposed by Lindholm and Yeakley (1968). In this design, a "top hat" specimen is sandwiched between the incident bar and a hollow transmission tube. Figure 8.4 shows a configuration of this design. The compression stress waves in the incident bar strike the inside of the specimen hat, which causes a tensile load on the specimen gage section. The stress wave then propagates into the transmission tube in compression. To increase the stress amplitude in the specimen, the specimen gage section was not entirely solid. Lindholm and Yeakley (1968) split their tube portion of the hat specimen into four arms with a length to width ratio of 2. Using a specimen hat has minimal modifications to the Kolsky compression bar and does not require attaching the specimen to the bar ends which typically involves threading both the specimen and bar ends. By placing different specimens on the side of hat-shaped specimen section, Lindholm and Yeakley's design also accommodates the testing of multiple specimens in one experiment. Mohr and Gary (2007) recently proposed an M-shaped specimen that uses a compression bar to apply dynamic tensile load on small specimens.

Nicholas (1981) proposed a very clever way of utilizing a compression bar to perform tensile experiments. His design is schematically shown in Fig. 8.5. A specimen is threaded onto the ends of the incident and transmission bar in the test section. A rigid collar is placed over the specimen to allow the compression wave to pass through the collar and leave the specimen virtually untouched by the initial compression wave. The cross-sectional area of the collar is much larger than that of the specimen. Most of the compression energy in the incident bar due to the impact of striker is transferred into the transmission bar. When the com-

pression stress wave travels to the free end of the transmission bar, it is reflected back as a tensile wave propagating back towards the specimen. When this tensile wave arrives at the specimen, the rigid collar cannot support the tensile wave and the specimen is subjected to a dynamic tensile pulse. Nicholas' setup uses a conventional Kolsky compression bar setup of 4130 steel with the ends being heat treated to about Rc47 to ensure that the ends would not deform during loading. This method involves minimum modifications to the existing Kolsky compression bar. The only modifications are to thread the bar ends and to make a rigid collar. However, the specimen in this design is inevitably subjected to compression before tension even though the collar is used.

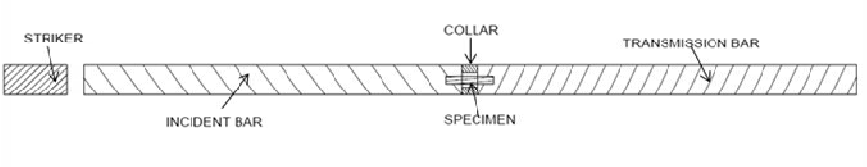

Figure 8.5 Generation of tensile load using compression wave reflection

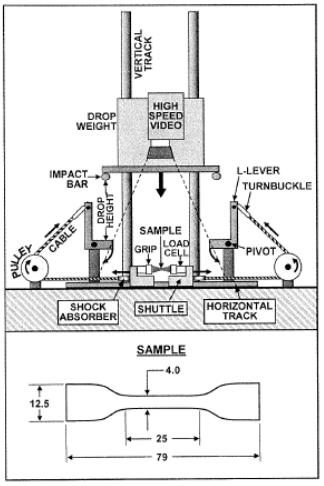

Figure 8.6 A drop-weight driven tensile tester
(Reproduced from Mott et al. (2007) with permission)

At lower rates, Mott et al. (2007) modified a drop tower with a pulley system to test elastomers at strain rates of 10 to 1600 s^{-1}. The setup drops a 100 kg weight onto an L-lever. A set of impact bars are attached to the drop weight plate in order to allow the lever to rotate and to attain line contact with the L-lever system (Fig. 8.6). The L-lever is allowed to pivot using low friction bearings; it is also connected to a pulley system that in turn connects to a shuttle piece. The shuttle piece grips onto the sample and subjects the sample to tensile loading. It is critical that the L-lever system is aligned meticulously in order to accommodate even loading.

The most commonly used loading method in a Kolsky tension bar is direct tension. Similar to the compression case, there are two main types of direct tension methods. One is to store elastic energy by stretching a section of the incident bar in tension (Staab and Gilat 1991; Cadoni et al. 2009). The section begins at the far end (from the specimen) of the incident bar. A clamp divides the pre-stressed and stress-free sections. The sudden release of the clamp allows the release of stored energy in the form of tensile stress waves, which propagate towards the specimen and load it dynamically in tension. Figure 8.7 shows a system using stored energy (Cadoni et al. 2009). In this setup, a pre-stressed bar is used to store the tensile elastic energy. The sudden breaking of a brittle intermediate piece results in a tensile wave in the incident bar. The brittle blocking piece may be a clamp with a sudden-release feature. In such a system, the way the brittle piece breaks or the clamp releases is difficult to control. Therefore, pulse shaping in these systems is not feasible.

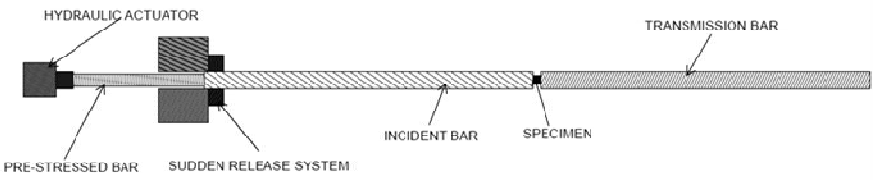

Figure 8.7 Generating a tensile pulse using stored energy

The other approach to generate direct tension in the incident bar is to strike a flange at the end of the incident bar with a form of kinetic energy. One approach to generate the kinetic energy is to use a rotating disk loading system with impact hammers (Kawata et al. 1979). Figure 8.8 show a schematic of such a loading system in a Kolsky tension bar.

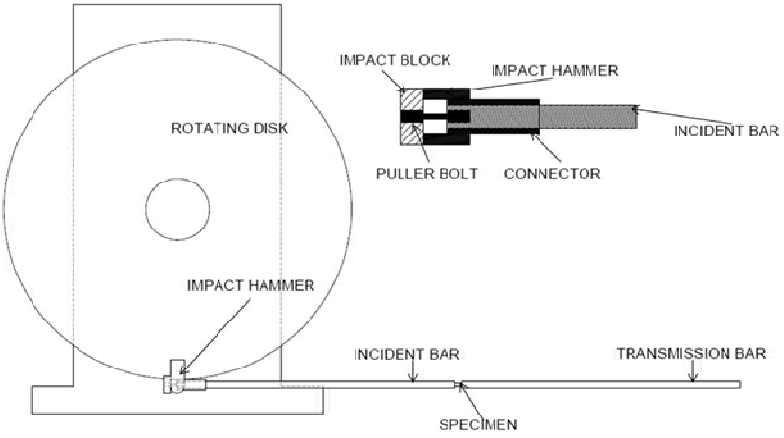

Figure 8.8 A rotating-disk loading system on a tension bar
(Reproduced from Kawata et al. (1979) with permission)

Before the disk is accelerated, the hammers are retracted into the disk through a caging device. An electromagnetic controller releases the hammers when the disk is rotating at the desired speed, subjecting the hammers to impact on the block which is connected to the incident bar with a prefixed metal bar, as shown in Fig. 8.8. The prefixed metal bar is thus stretched to fracture, generating a tensile pulse in the incident bar. The prefixed metal bar provides a means for pulse shaping. With the proper use of the material and geometry of the bar, the shape of the incident pulse can be controlled to some extent. Figure 8.9 shows a similar system with a more elaborate design for waves traveling in the incident bar after the hammer impact (Li et al., 1993). This tensile setup can actu-

ally conduct dynamic experiments under single and multiple tension loads.

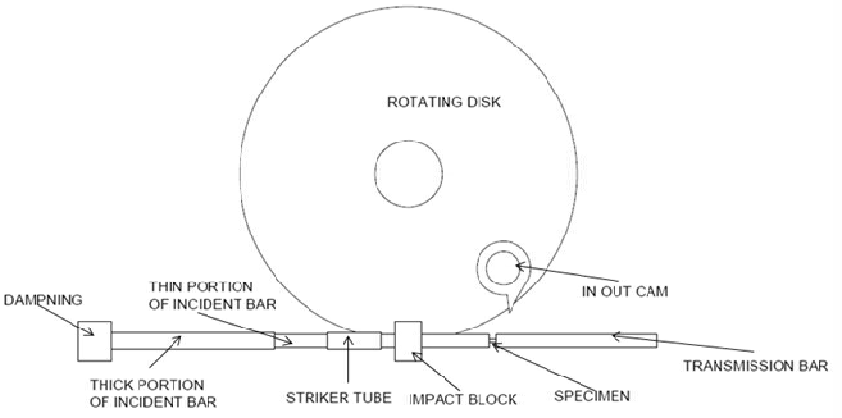

Figure 8.9 A rotating-disk bar for tension and tension-tension loads
(Reproduced from Li et al. (1993) with permission)

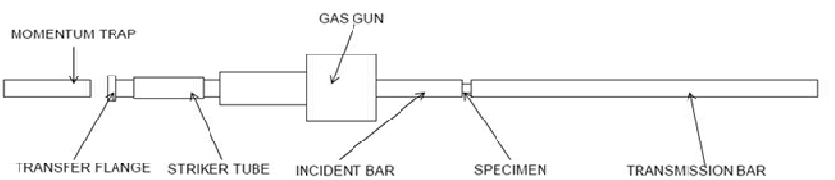

Figure 8.10 A direct impact tension bar

Another direct loading method is to drive a tubular striker by either a gas gun or a spring system. The tube slides on the incident bar. When the tube impacts on a flange at the end of the incident bar, a tensile pulse is generated in the incident bar and propagates to the specimen. Except for the tubular striker and the tensile test section, this method is similar to the Kolsky compression bar. Figure 8.10 shows a schematic of such a system. The gas gun chamber can be designed to envelope the bar, as shown in Fig. 8.10, or on the side of the bar as shown in Fig. 8.11 (Owens and Tippur 2009). The momentum trapper on the left side provides the possibility for single-loading capability on the specimen when the gap between the trapper and the flange on the incident bar is properly set. The gap should close after the generation of the first incident pulse, as illustrated in Fig. 2.25 (Nemat-Nasser et al. 1991). The impact surfaces between the striker and the flange provide a platform for placing pulse shapers that control the profiles of the incident pulses.

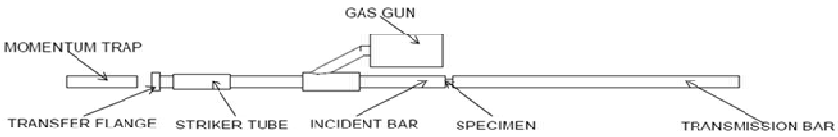

Figure 8.11 A different design of the direct-impact tension bar
(Reproduced from Owens and Tippur (2009) with permission)

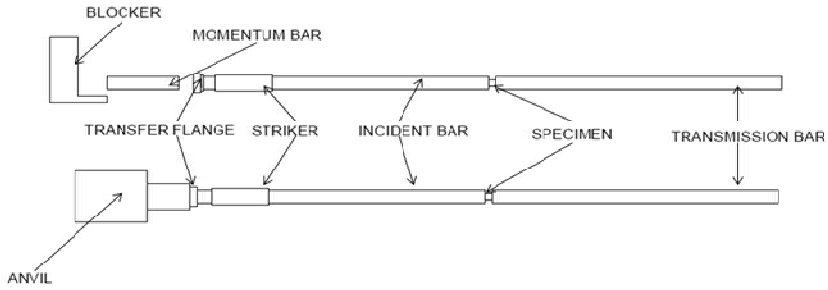

Figure 8.12 A direct impact tension bar for multiple loading
(Reproduced from Ogawa (1984) with permission)

The interface between the flange and the momentum trapper provides another platform for controlling loading pulses. Figure 8.12 shows a design for the momentum-trapping system that, when properly arranged, can load the specimen with multiple loads such as tension-tension and tension-compression-tension (Ogawa 1984). The desired loading conditions were achieved by the employment of a momentum bar or an anvil that controlled the impedance mismatch between the incident bar and the momentum-control devices. The second loading pulse arriving at the specimen was either tension or compression.

In the design shown in Fig. 8.13, the momentum-control device is a massive bar to divert most of the impact force to the trapper (Nie et al. 2009). The purpose is to strike the flange at velocities sufficiently high for consistency while generating a low-amplitude incident pulse for loading a soft specimen. The design in Fig. 8.13 also uses a compound incident bar where an aluminum bar with a smaller diameter (smaller impedance) connects to the initial steel portion of the incident bar. This connection reflects part of the low-amplitude incident pulse back into the steel portion of the incident bar, further reducing the amplitude of the incident pulse that propagates along the aluminum bar to the soft specimen.

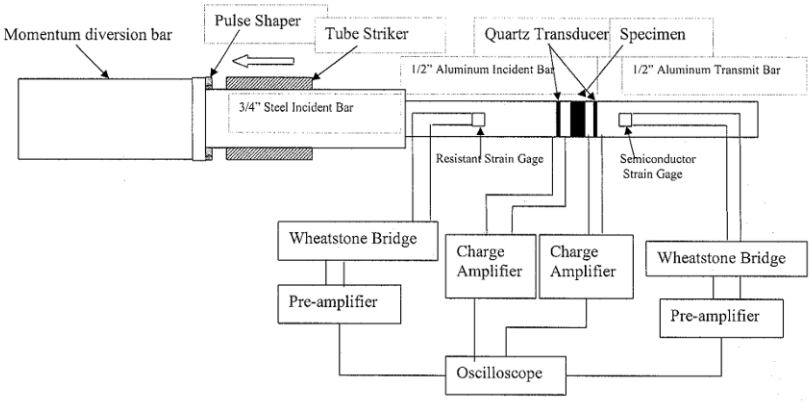

Figure 8.13 A tension bar for soft specimens
(Reproduced from Nie et al. (2009) with permission)

8.2 Tension Specimen Design

The design considerations for tension specimens are similar to compression specimen in terms of dynamic equilibrium and the strength limit of the Kolsky bars. In tension experiment design, there are more factors that need to be taken into account. The largest variation from compression experiments is that the specimen must be firmly connected to the bar ends in tensile experiments. The joint between the specimen and the bars may be clamped, threaded, bonded, or specially gripped. The clamped joint is used mostly for materials that are difficult to thread or bond, for example, soft tissues or polymers. Figure 8.14 shows the clamping system to attach a rubber specimen to the tension bar ends. The specimen is a sheet that is wrapped around the bar ends and then clamped to the bars. The inner surface of the clamp is artificially made rough to improve the clamping and to prevent uneven shear deformation over the specimen thickness in the clamped area (Nie et al. 2009).

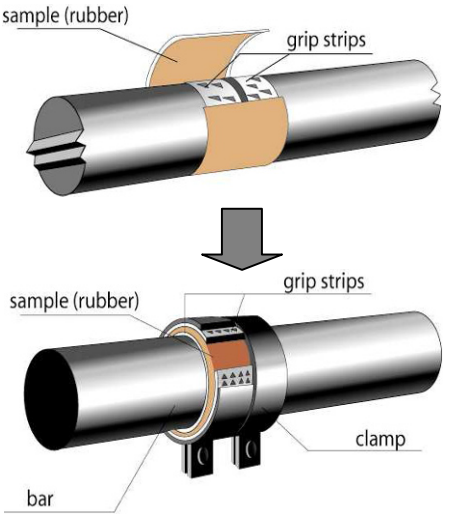

Figure 8.14 A clamped tension specimen
(Reproduced from Nie et al. (2009) with permission)

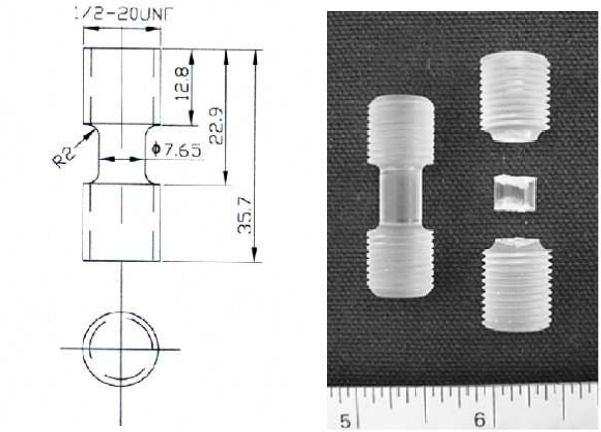

Figure 8.15 A threaded tension specimen
(Reproduced from Chen et al. (2002a) with permission)

Figure 8.15 shows the geometry of a glassy polymer tension specimen before and after dynamic failure. The specimen was tested using a 19-mm diameter Kolsky tension bar with female ½-20 threads on the bar ends (Chen et al. 2002a). The fillet design between the threaded section and the gage section of the specimen is critical to minimize stress concentrations in the specimen. For specimens that are not suitable to be wrapped or threaded, for example flat composite coupons, bonded joint becomes a popular choice. The flat specimen is fit into slots at the bar ends and glued. If the specimen has specific mounting requirements, adaptors can be made to connect the specimen to the bar ends. Figure 8.16 shows an example of a cement tension specimen, which is glued to adaptors at the bar ends. The glued joint ensures that there is no slippage during the dynamic tensile loading. However, it is experimentally not efficient to remove the specimen from the bonded joints after mechanical loading.

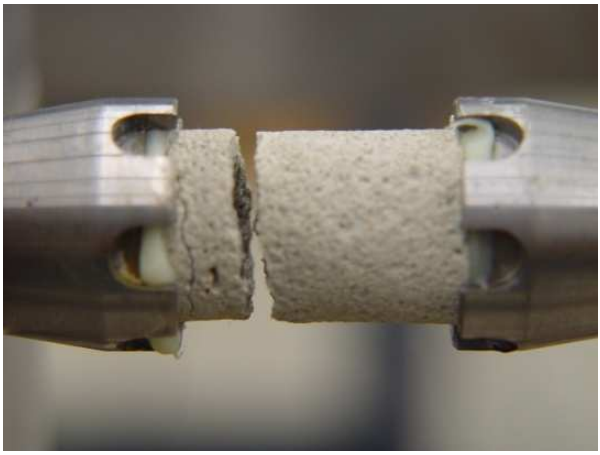

Figure 8.16 A cement tension specimen glued to adaptors

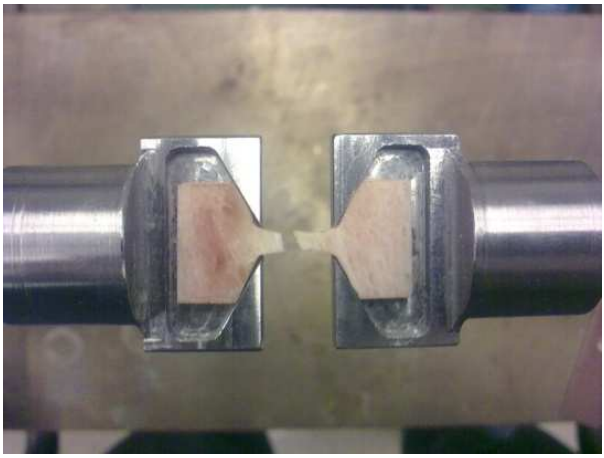

Figure 8.17 A pair of special grips for bone specimen in tension

Some of the tensile specimens have additional gripping requirements where grips with specific purposes are designed. As an example, Fig. 8.17 shows a pair of tension grips that hold a bone specimen. Like most biological tissue specimens, the mechanical response of bone specimens depends on the time duration from the termination of animal to specimen preparation and then to mechanical testing. The properties also depend on the way the samples are preserved before mechanical loading. Due to the time to cure, glued joint is typically not acceptable in the experiments on these materials. The special grips shown in Fig. 8.17 facilitate fast specimen installation and replacement.

Due to the dynamic equilibrium requirements, the specimen length is limited. Therefore, the end effects are more severe in these specimens. Furthermore, the strain rate in the specimen is calculated by the difference between the bar-end velocities divided by the specimen length. In the case of the dumbbell-shaped tension specimens, the gage length is not well determined. The deformation of transition regions of the specimen may be counted as the gage-section deformation, which leads to an over-estimated specimen strain. In the elastic deformation range, Albertini and Montagnani (1977) suggested a way to correct the strain in the specimen,

$$\varepsilon = \varepsilon_m - \sigma \frac{E - E_m}{E E_m} \tag{8.1}$$

where ε_m and σ are calculated from raw data using (1.13) and (1.14), respectively. The specimen length is taken as the length of the gage section. E_m is the measured Young's modulus, which is typically lower than the actual value E. For most metallic and ceramic materials, the value of E does not vary from quasi-static to Kolsky bar strain rates.

Despite such artificial correction measures, the unknown end-effect zone and the vague gage length form a major concern for uncertainties in the data reduction for strain-rate and strain histories in the tension specimen. For this reason, strain measurements directly from specimen surface are preferred. For example in a brittle specimen, a strain gage is mounted on the surface of the specimen gage section as an effective method. For specimen materials that deform to larger strains, optical methods provide more accurate measurements.

One optical method is digital image correlation (DIC) which proves to be very effective (Gilat et al. 2009). Both 2-D and 3-D full field specimen surface deformation histories can be recorded and analyzed using this method. The 2-D strain fields can be imaged by one camera with its optical axis perpendicular to the plane of deformation. By contrast,

the 3-D strain fields need images taken from two different angles and can be imaged either by two synchronized high-speed digital cameras or by projecting images from two directions to different portions of one camera aperture. The experiment is performed the same way as a regular Kolsky tension bar test with the gage section accessible for optical camera access. The specimen surface is prepared with a random pattern for automatic position tracking. A high-speed camera is triggered when the specimen starts to deform and records the deformation process. For typical Kolsky bar experiments, the camera speed needs to be around 80,000 to 300,000 frames per second. A DIC analysis then tracks the motion of the random dots on the pattern and calculates the progressive full-field displacement and strain fields. With the known imaging frame rate, the strain rate can be determined. This method provides direct strain measurement over the entire specimen surface. In addition, the end-effect zone may be visible from the images.

8.3 Pulse Shaping in Tension Experiments

Similar to compression experiments, the desired profiles of the incident pulses are determined by the specimen response and intended loading conditions on the specimen such as strain rate and ultimate strain. Unlike compression experiments where the impact surface of the incident bar is available to attach well-designed pulse shapers to tailor the incident pulses, the impact surface is not available (in the cases of pre-stressed bars) or very limited (in the cases of rotating wheel and tubular impact). Only limited pulse-shaping efforts have been reported based on trial-and-error approaches (Chen et al. 2002, Nie et al. 2009). A new design that can fully utilize the compression pulse-shaper techniques is emerging (Guzman et al. 2010, Song et al. 2010).

8.4 Methods to Generate Dynamic Torque

Compared to the Kolsky compression and tension bars, the torsion version of the Kolsky bar eliminates the radial inertia effects in the bars. Therefore a torsion test is most closely described by one-dimensional stress wave theory since the wave propagation in the elastic bars is non-

dispersive. Baker and Yew (1966) developed the original torsion bar on top of a lathe. Figure 8.18 is a schematic of this design.

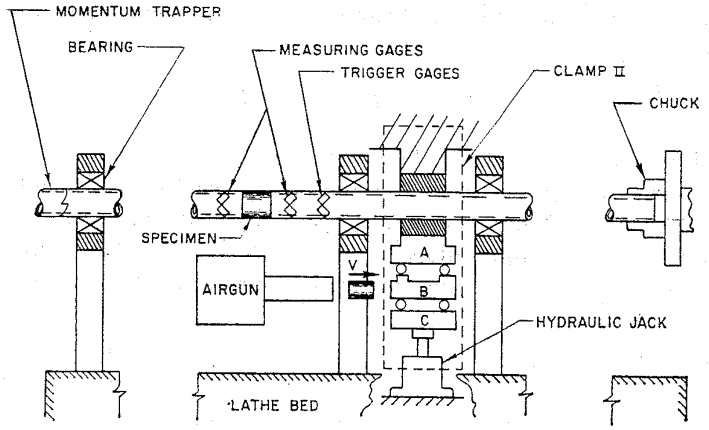

Figure 8.18 Baker and Yew's design of Kolsky torsion bar
(Reproduced from Baker and Yew (1966) with permission)

This design has similarities to the pre-stressed versions of the tension bars. As shown in Fig. 8.18, the lathe chuck clamps on the loading end of the incident bar on the right side of the figure. A hydraulic clamp holds the incident bar at a selected location. The section of the incident bar between the clamp and the chuck will be pre-stressed in torsion. The length of this section depends on the needed duration of the loading pulse. The specimen is a thin tube which was brazed to the incident and transmission bars. The far end of the transmission bar is connected to a momentum trapper through a one-direction jaw. During an experiment, the pre-stressed section is twisted by the chuck within the elastic range of the incident bar. The clamp is then suddenly released by shooting a projectile against a movable link in the clamp system (Fig. 8.18). This lets the torsional strain energy to propagate towards the specimen in the form of one-dimensional shear wave. When the shear wave arrives at the specimen, part of the wave is reflected back due to impedance mismatch between the bar and the specimen and the rest propagates through the

specimen into the transmission bar. The surface strains associated with the waves are recorded using the surface strain gages mounted 45° from the axial direction. The data analysis is the same as in the compression or tension bars.

Duffy et al. later (1971) used explosive loading to initiate the one-dimensional torsion waves in the incident bar. They used copper pulse smoother to filter out the high-frequency components in the initial torsion wave generated by the detonation of the explosive, which is the first documented effort for pulse shaping. Most torsion bars use mechanical methods to store torsional strain energy in a pre-stressed section of the incident bar similar to Baker and Yew (1966). The torque generator may be a simple pulley or a hydraulic rotation actuator. Figure 8.19 shows a schematic of a typical torsion bar setup where the clamp is also shown in detail.

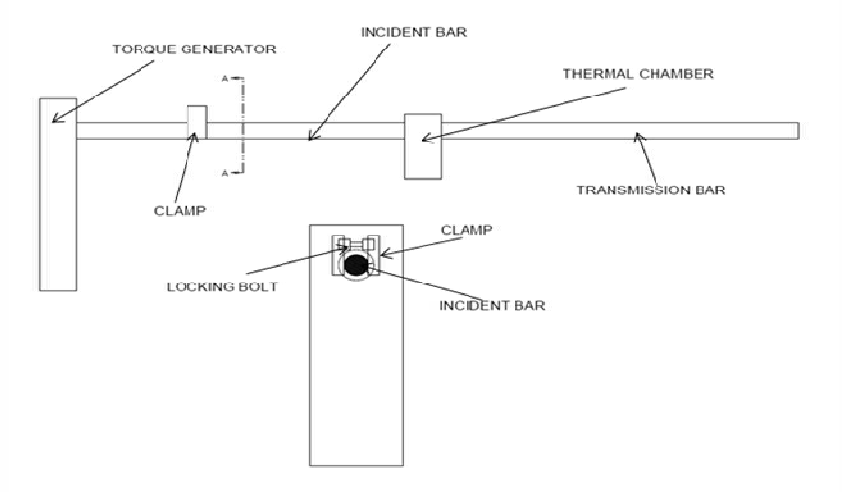

Figure 8.19 A typical torsion bar

In the setup shown in Fig. 8.19, a torque generator (mechanically driven pully) is used to twist the incident bar between the pulley and the clamp position (marked A-A). The clamp consists of two side columns with the incident bar in between. The tops of the columns are connected by a locking bolt (pin) that has a very sharp notch in the middle (see A-A View). The incident bar is clamped in the middle. The clamping force is provided by a hydraulic actuator near the bottom. When the actuator is in action, the bar is compressed across its diameter, and the locking pin is in tension. The initial clamping force should be sufficiently high such that the incident bar is firmly clamped without any slip when the torque is applied. However, the initial clamping force should not break the locking pin. When the torque is at a desired level (determined by the intended strain rate and specimen response), further clamping force is applied by the hydraulic actuator. The increasing clamping force produces increasing tensile load in the locking pin until the pin fails suddenly at the sharp notch. The torque then transmits into the incident bar in the form of torsion wave. To generate a clean incident pulse, the material for the locking pin should have a brittle fracture, such as cast iron or strong aluminum alloys.

8.5 Torsion Specimen Design

Since there exists strain gradient along the radius of a cylinder under twist, the specimen in a torsion bar experiment is typically a thin tube to approach uniform strain in the gage section. The typical specimen designs for torsion experiments are shown in Fig. 8.20 (Hartley et al. 1987). Both have short and thin-walled central gage sections. The specimen on the left side has circular flanges that can be bonded to the bar ends. The large area of the flanges provides sufficient bond area to support the torsion load necessary to deform the much-smaller gage section plastically. The advantage of the circular flanges is that the impedance of the specimen in this portion can be matched with that of the bars, which minimizes disturbances to the one-dimensional wave propagation through the bars. If the specimen material has a high strength that overcomes the bond interface strength, this specimen design will not be applicable any longer. Instead, hexagonal (as seen on the right side of Fig. 8.20), or square flanges should be used as they can be firmly clamped by the recesses in the bar ends with matching shapes. In addition to dynamic shear stress-strain curves, the outside of the specimen gage sections can

be marked and high-speed imaged to study shear localization under high-rate loading conditions.

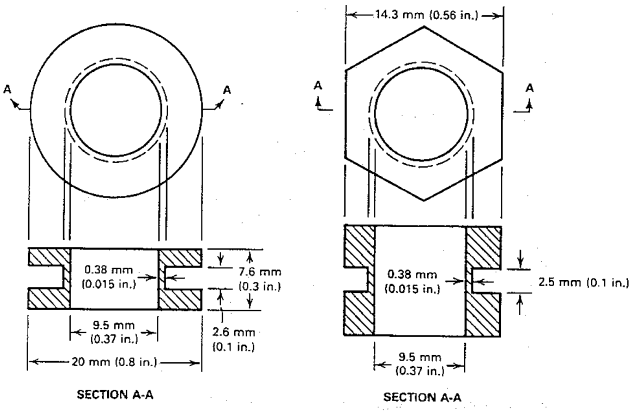

Figure 8.20 Shear specimen geometry
(Reproduced from Hartley et al. (1987) with permission)

8.6 Combined Axial/Torsion Loading

The Kolsky torsion bars with a pre-stressed section are readily modified to conduct dynamic experiments on specimens with combined axial and torsion loading. The pre-stress section is not limited in one type of stored strain energy. For example, when the bar is clamped at its claming location, a pulley may be used to twist the bar to store torsional strain energy in the pre-stressed section. Meanwhile, a hydraulic actuator may also be introduced to induce tensile or compressive strain energy in the same pre-stressed section. The sudden release of the clamp thus generates two types of elastic waves in the incident bar simultaneously, which is tension or compression, in addition to shear. However, the shear wave will arrive at the specimen behind the axial wave due the differences in wave speeds.

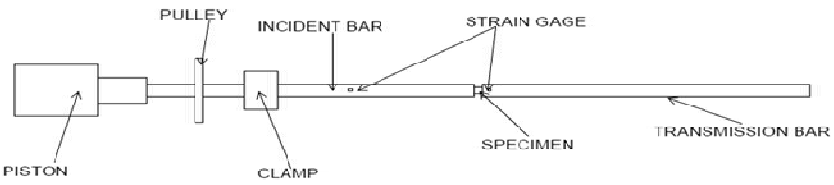

Figure 8.21 A compression/torsion bar for dynamic friction study
(Reproduced from Huang and Feng (2004) with permission)

Figure 8.21 schematically shows a compression/torsion bar for dynamic friction studies (Huang and Feng 2004). To investigate the friction behavior on an interface, normal pressure with a controllable amplitude is required across the interface before a shear load is applied to determine the friction coefficient. This loading pattern is exactly what the device shown in Fig. 8.21 can provide. Similar designs have been used to study dynamic friction (Rajagopalan and Prakash 1999, Espinosa et al. 2000).

8.7 Examples of Dynamic Tensile Experiments

8.7.1 Epoxy and PMMA

In this section, the dynamic stress-strain responses and failure behavior of an epoxy, Epon 828/T-403, and a PMMA are tested under high strain-rate uniaxial tension conditions. The Kolsky-bar setup for high-rate tension experiments is schematically shown in Fig. 8.22. The striker is a tube sliding outside the incident bar. In order to increase the magnitude of the weak transmitted signal, an aluminum alloy tube was used as the transmission bar. At the specimen-transmission bar interface, an aluminum alloy end cap was press-fit and then welded onto the hollow tube to provide a threaded grip for the specimen. This end cap could disturb the one-dimensional wave propagation in the aluminum tube. However a pulse-shaper is used to control the profile of the incident pulse with a substantially increased rise-time and to filter out high-frequency components in the waveform, so that the cap is in dynamic equilibrium together

with the specimen. The pulse shaper is necessary anyway to facilitate dynamic stress equilibrium and constant strain rate in the polymer specimen with low wave speeds.

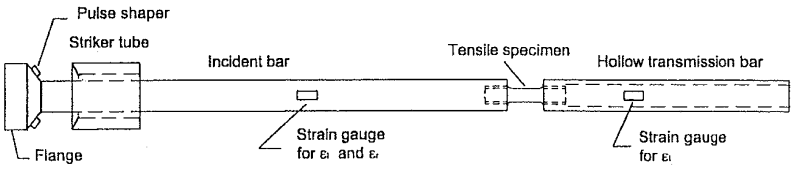

Figure 8.22 The experimental setup for dynamic polymer tension tests
(Reproduced from Chen et al. (2002) with permission)

With the solid steel incident bar and hollow aluminum transmission bar, the strain calculation needs to account for the change in the relationship between the bar-end velocity and the measured strain signal on the tube. The tensile strain history in the specimen is

$$\varepsilon(t)=\left(\frac{C_{BI}}{L_S}-\frac{E_I A_I}{E_T A_T}\frac{C_{BT}}{L_S}\right)\int_0^t \varepsilon_i(\tau)d\tau-\left(\frac{C_{BI}}{L_S}+\frac{E_I A_I}{E_T A_T}\frac{C_{BT}}{L_S}\right)\int_0^t \varepsilon_r(\tau)d\tau \tag{8.2}$$

where subscripts I and T represent the incident bar and the hollow transmission tube, respectively. For the modified tension bar used for the experiments presented, the lengths of the maraging steel striker tube and incident bar were 152 and 2130 mm, respectively, and the length of the 6061-T6 aluminum hollow transmission tube was 762 mm. They all had a common outer diameter of 19 mm. The inner diameter of the transmission tube was 16 mm.

The specimen materials are two amorphous polymers, an amine-cured DGEBA epoxy (Shell Epon 828 epoxy resin with a Texaco T-403 hardener using a 100/36 weight ratio) and a PMMA. The epoxy with a mass density of 1.14×10^3 kg/m^3 and a glass transition temperature of 55°C was cured at room temperature for over seven days. The PMMA

was purchased from a commercial vender. The specimens were then machined to a dumbbell shape with the dimensions specified in Fig. 8.15. The specimen length was determined by trial tests to check dynamic stress equilibrium in the specimens. Before dynamic loading, all the Epon epoxy specimens were heated in a sealed container in a furnace to 60°C, kept at that temperature for four hours, and cooled down to room temperature overnight. The same procedure was repeated on PMMA specimens except that the annealing temperature was 110°C. This procedure was designed to relieve any residual stress in the specimens from material handling and machining.

Uniaxial tension experiments on the epoxy were performed using the modified Kolsky tension bar. To explore the rate effects over a wider range, quasi-static tension experiments were also performed. The tensile response was obtained at four strain rates: $2.46\times10^{-3}\,s^{-1}$, $2.26\times10^{-1}\,s^{-1}$, $8.0\times10^{2}\,s^{-1}$, and $1.2\times10^{3}\,s^{-1}$ (Chen et al. 2002a). The tensile stress-strain curves are shown in Fig. 8.23.

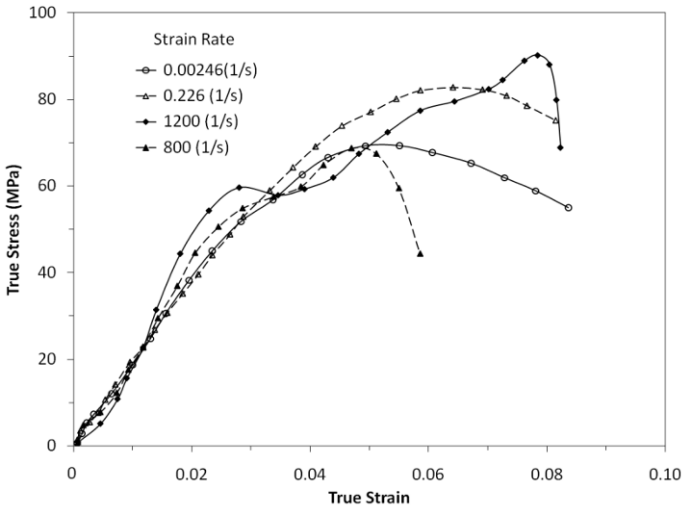

Figure 8.23 Tensile stress-strain curves of Epon 828/T-403 epoxy
(Reproduced from Chen et al. (2002a) with permission)

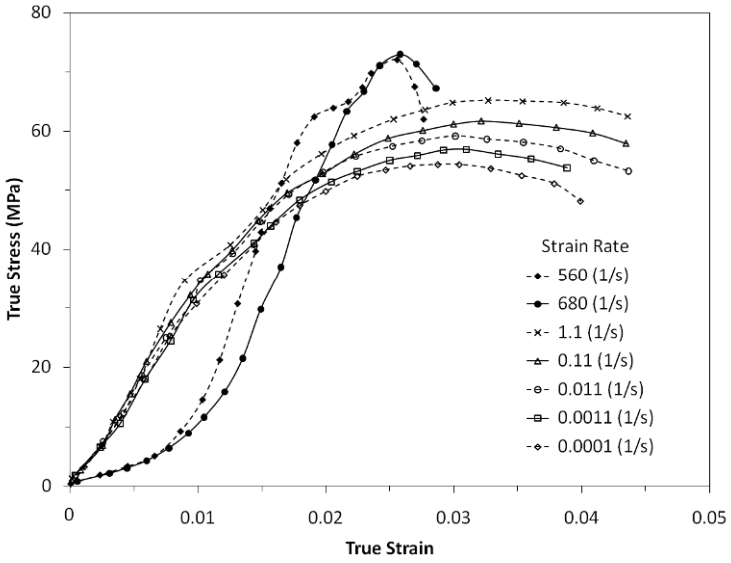

Figure 8.24 Tensile stress-strain curves of PMMA
(Reproduced from Chen et al. (2002a) with permission)

The results shown in Fig. 8.23 indicate that the peak strength was reached during a dynamic test at a smaller strain as compared to quasi-static tests. The results in Fig. 8.23 do not show clear strain-rate dependence of the material's peak tensile strength, which is in contrast to the rate sensitivity in compression of this material (Chen and Zhou 1998). The specimens fractured in a brittle manner during dynamic tensile loading, which is consistent with the smaller failure strains. By contrast, during quasi-static tension tests, these specimens failed in a ductile manner with a necking process. The brittle-ductile transition is considered to be the strain-rate effect. The fact that more than one fracture-surface exist, as shown in Fig. 8.15, indicates that dynamic stress equilibrium had been reached before fracture occurred. However, the fracture was near the fillets, which indicts that stress concentration near the fillets played a role. Ideally, the fracture should occur near the middle of the gage section.

Figure 8.24 summarizes the tensile stress-strain curves of the PMMA over a strain-rate range of 1.0×10^{-4} to 6.8×10^{2} s^{-1}. Similar to the behavior of Epon 828/T-403, the results Fig. 8.24 indicate that the strain

corresponding to the peak strength in dynamic experiments is smaller than that from quasi-static experiments. The peak tensile strength under dynamic loading is slightly higher than its quasi-static counterpart of the material. Similar to the behavior of Epon epoxy, the specimens failed in a ductile manner with a necking process during quasi-static tests. However, under dynamic tensile loading, the failure changed to a brittle fracture manner. The initial toe region of the dynamic tensile stress-strain curves may come from the engagement process of the threaded joints between the specimen and the bar ends.

8.7.2 Bovine Tendon

In this example, a Kolsky tension bar was used to determine the tensile stress-stretch behavior of the bovine tendon under dynamic loading (Cheng et al. 2009). Dynamic Mullins effects on the tendon stress-strain response were also explored. The tendon specimens can deform to large strains. To properly hold the tendon specimen without slipping during tensile loading, grips similar to the 'cryo-jaw' device (Cheng and Chen 2003) were used. This gripping method introduced minimum disturbances to the stress wave propagations in the Kolsky tension bar. To translate the testing machine crosshead displacement into the actual strains in the gage section of the specimen, Miller's (2001) equation was employed for the specific specimen configuration of rectangular cross section used in this research (Cheng and Chen 2003). A laser displacement measurement device was used to measure the actual strain history in the specimen. The device includes a laser diode, a line head, and a photo detector. The details and working principles of the laser device are given by Ramesh and Narasimhan (1996). The only difference is that the device was turned by 90° from Ramesh and Narasimhan's design to measure the width changing of an opening gap. Since the tendons are of relatively weak strength, a hollow transmission bar was again used to accurately measure the transmitted force signal. To achieve early stress equilibrium and a constant strain rate in the specimen, pulse-shaping was employed. Furthermore, to evaluate the Mullins effects under dynamic loading conditions, it is important for the specimen to be loaded only once during one loading cycle. A momentum trapping bar was used to prevent undesired repeated pulses. A schematic illustration of the dynamic experimental setup is shown in Fig. 8.25.

The tendon specimens used in this set of experiments had rectangular cross-sections. Four specimens were excised from one tendon segment, as shown in Fig. 8.26. The specimens were then kept hydrated for tests. The gauge section of the specimens was 3×2 mm^2 in cross-sectional area and 8 mm in length.

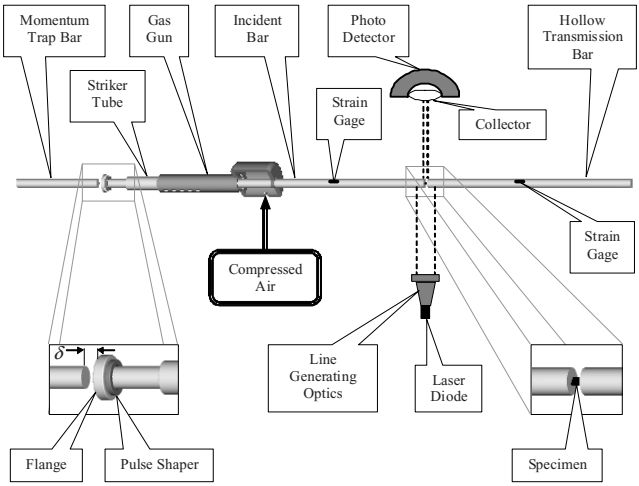

Figure 8.25 A Kolsky tension bar for tendon tension experiments
(Reproduced from Cheng et al. (2009) with permission)

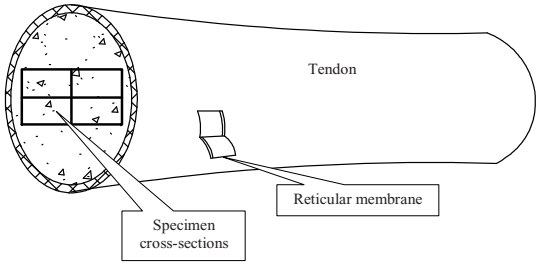

Figure 8.26 Tendon tension specimen preparation
(Reproduced from Cheng et al. (2009) with permission)

Figure 8.27 shows the dynamic stress-strain behavior of the tendon specimen over three loading cycles. Since it is difficult to completely eliminate the repeated loading from the tension bar setup used in this study, the actual maximum strain of the first impact experiment is about 0.20. The subsequent loading paths are well below the first one and gradually approach a stable path. The differences between the stress-stretch curves from different loading cycles are similar to the Mullins effects observed in rubbers under quasi-static cyclic loading conditions. Similar phenomena were also observed when the tendon was loaded repeatedly under quasi-static rates, although the dynamic stress-stretch curves have higher slopes than their quasi-static counterparts. These results show that the mechanical responses of tendons depend on the loading history and strain rate. The stress-strain response of a fresh tendon (such as the one marked by "1st loading" in Fig. 8.27) is quite different from an exercised tendon (such as the other two curves in Fig. 8.27), under both quasi-static and dynamic loading conditions. The peak stresses of the curves in Fig. 8.27 correspond to the start of unloading in each experiment.

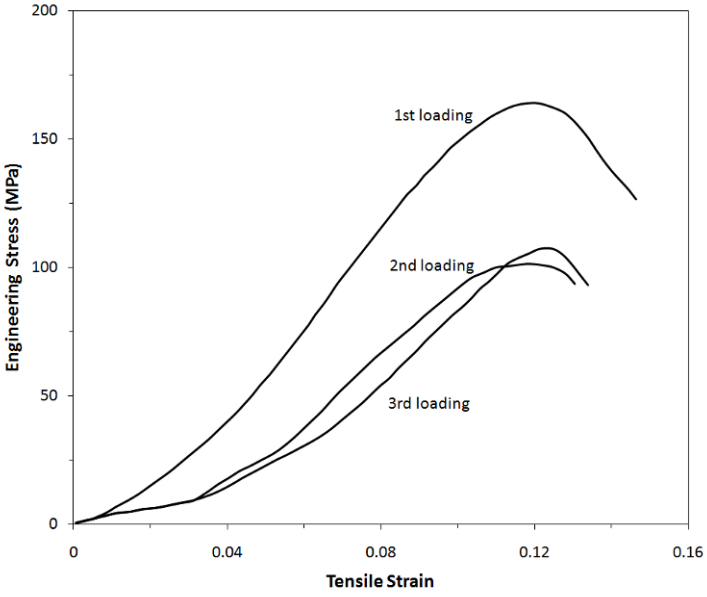

Figure 8.27 Dynamic tensile stress-strain curves of bovine tendon at a strain rate of 2500 s^{-1}

(Reproduced from Cheng et al. (2009) with permission)

8.7.3 Rubber

Dynamic tensile response of the EPDM rubber presented in Chapter 4.5.2.3 was determined using a modified Kolsky tension bar. The soft sheet specimen was wrapped around the ends of the aluminum bars to form a tubular geometry, as shown in Fig. 8.14. The inner surface of the tube was glued to the cylindrical surfaces of the bar ends. The outer surface of the specimen was clamped. Trial experiments were performed to select clamps that introduced minimum disturbances to the wave propagations in the bars. Thin metal liners with rough surfaces were attached to both the bar surface and the inner surface of the clamp such that shear deformation in the specimen during tension is minimized. This specimen geometry minimizes not only 3-D stress state but also radial inertia effects. Similar to Kolsky compression bar experiments, the quartz-crystals required for equilibrium checking in soft material testing are located near the bar ends.

The tension bar used in this study is schematically shown in Fig. 8.13. It consists of a momentum diversion bar, a compound incident bar, a tubular striker, and a transmission bar. The 25.4 mm diameter steel momentum diversion bar has a length of 2692 mm. The 2286-mm long steel section of the incident bar has a diameter of 19.0 mm and the 1830-mm long aluminum section has a diameter of 12.7 mm. The 12.7 mm aluminum transmission bar is 1830-mm long. The steel tubular striker, which rides on the steel portion of the incident bar, has the same cross-sectional area as the steel incident bar and is 533-mm long. During an experiment, the momentum diversion bar is in contact with the flange at the end of the incident bar. The tubular striker is driven by a gas gun towards the flange-end of the incident bar and impacts against the flange. Upon impact, the momentum diversion bar absorbs most of the impact energy because of its larger cross-sectional area. The stress in the steel portion of the incident bar, σ_I, induced by the impact of the striker traveling at an initial velocity V_0, is

$$\sigma_I = \frac{\rho_B C_B V_0 A_I}{2A_I + A_M} \tag{8.3}$$

where V_0 is the striking velocity of the tubular striker; and A_I and A_M are the cross-sectional area of the striker, which is the same as that of the steel section of the incident bar, and the momentum diversion bar, respectively. With the dimension described above, the incident bar stress

amplitude reduces by nearly 47% after the momentum diversion bar is used. As the incident tensile pulse further propagates to the steel/aluminum joint of the incident bar, the stress in the aluminum section of the incident bar, σ_a, is

$$\sigma_a = 2\frac{A_I}{A_a}\frac{1}{1+R}\sigma_I \tag{8.4}$$

where A_a is the cross-section area of the aluminum section, $R = \frac{\rho C A_I}{\rho_a C_a A_a}$ is impedance ratio between the steel and the aluminum sections of the incident bar. With the experimental setup used in this study, σ_a is about 60% of σ_I. Thus, with the momentum diversion bar and the steel/aluminum joint, the amplitude of the incident stress is only about 1/3 of that produced in a conventional tension bar. This allows much higher striking velocities to generate relatively low but repeatable incident stress pulses needed for soft material testing.

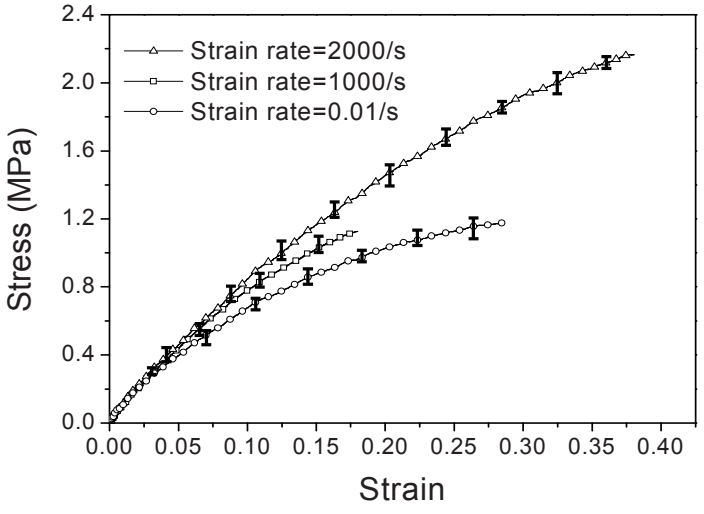

Figure 8.28 Tensile stress-strain curves of EPDM rubber at various strain rates

(Reproduced from Nie et al. (2009) with permission)

Figure 8.28 shows the dynamic tensile stress-strain curves of the EPDM rubber at two different high strain rates and a reference quasi-static strain rate (Nie et al. 2009). Each stress-strain curve presented in the figure is the mean curve of five experiments conducted under identical loading conditions. Error bars are also shown on each curve to indicate the scattering range of the stress-strain curves obtained under each identical loading condition. The tensile stress-strain curves of the EPDM exhibit non-linear behavior with significant strain-rate dependency, which is a characteristic of typical viscoelastic materials. In comparison to its compressive response presented in Chapter 4.5.2.3, the EPDM is softer in tension.